

# Evaluation of errors from neglecting polarization in the forward modeling of O<sub>2</sub> A band measurements from space, with relevance to CO<sub>2</sub> column retrieval from polarization-sensitive instruments

Vijay Natraj<sup>a,\*</sup>, Robert J.D. Spurr<sup>b</sup>, Hartmut Boesch<sup>c</sup>, Yibo Jiang<sup>c</sup>, Yuk L. Yung<sup>a</sup>

<sup>a</sup>*Division of Geological and Planetary Sciences, MC 150-21, California Institute of Technology,  
1200 E. California Blvd., Pasadena, CA 91125, USA*

<sup>b</sup>*RT Solutions Inc., 9 Channing St., Cambridge, MA 02138, USA*

<sup>c</sup>*Jet Propulsion Laboratory, California Institute of Technology, 4800 Oak Grove Dr., Pasadena, CA 91109, USA*

Received 8 November 2005; accepted 6 February 2006

---

## Abstract

Sensitivity studies have been performed to evaluate the errors resulting from ignoring polarization in analyzing spectroscopic measurements of the O<sub>2</sub> A band from space, using the Orbiting Carbon Observatory (OCO) as a test case. An 11-layer atmosphere, with both gas and aerosol loading, and bounded from below by a lambertian reflecting surface, was used for the study. The numerical computations were performed with a plane-parallel vectorized discrete ordinate radiative transfer code. Beam and viewing geometry, surface reflectance and aerosol loading were varied one at a time to evaluate and understand the individual errors. Different behavior was observed in the line cores and the continuum because of the different paths taken by the photons in the two cases. The errors were largest when the solar zenith angle was high, and the aerosol loading and surface reflectance low. To understand the effect of neglecting polarization on CO<sub>2</sub> column retrievals, a linear error analysis study was performed on simulated measurements from the OCO spectral regions, viz. the 1.61 and 2.06 μm CO<sub>2</sub> bands and the O<sub>2</sub> A band. It was seen that neglecting polarization could introduce errors as high as 10 ppm, which is substantially larger than the required retrieval precision of ~2 ppm. A variety of approaches, including orders of scattering, spectral binning and the use of lookup tables are being explored to reduce the errors.

© 2006 Elsevier Ltd. All rights reserved.

*Keywords:* Reflected; Top of the atmosphere; Intensity; Polarization; Errors; O<sub>2</sub> A band; OCO

---

## 1. Introduction

The radiation reflected or transmitted by a planetary atmosphere contains information about the atmospheric constituents through their absorption and scattering signatures. Radiance measurements within gaseous absorption bands can thus be used to retrieve the vertical distribution of the absorbing gases, clouds

---

\*Corresponding author. Fax: +1 626 585 1917.

E-mail addresses: [vij@its.caltech.edu](mailto:vij@its.caltech.edu), [vijay@gps.caltech.edu](mailto:vijay@gps.caltech.edu) (V. Natraj).

and aerosols. In particular, the potential of spectroscopic observations of the O<sub>2</sub> *A* band to retrieve the surface pressure [1,2] and cloud top altitude [3–7] has been established.

Most remote sensing retrievals ignore the effect of polarization. While this is very often a very good approximation, there may be situations when measurements of polarization can provide additional information. Applications include retrieval of tropospheric ozone [8–11], cirrus clouds [12–14] and aerosols [15–18]. Polarized radiative transfer (RT) calculations are also important for the interpretation of satellite-based measurements such as from the Global Ozone Monitoring Experiment (GOME) [5,7,9–11,19] and the Scanning Imaging Absorption Spectrometer for Atmospheric Cartography (SCIAMACHY) [20–22]. Being UV instruments, where Rayleigh scattering is significant, they are sensitive to the polarization of the reflected radiation; hence, retrievals based on these measurements require consideration of polarization in addition to the intensity of the light incident on the detector.

Stam et al. [23] did a theoretical investigation of the behavior of the linear polarization of reflected and transmitted light in the O<sub>2</sub> *A* band for a few simple model atmospheres. They identified different regimes of behavior based on the gas absorption optical depth. In this paper, we take into account their findings and perform sensitivity studies to assess the effect of ignoring polarization on CO<sub>2</sub> column retrievals, using simulated measurements from polarization-sensitive space-based instruments, such as those to be acquired by the Orbiting Carbon Observatory (OCO) mission [24]. OCO will measure reflected sunlight in the near infrared absorption bands of CO<sub>2</sub> at 1.61 and 2.06 μm and the O<sub>2</sub> *A* band.

In Section 2, we give a brief description of vector RT theory. Details of the numerical model are discussed in Section 3. In Section 4, we elaborate on the atmospheric and surface setup, as well as the solar and viewing geometries. In Section 5, we use OCO as a test case and examine the effects of polarization on the upwelling radiance in the O<sub>2</sub> *A* band at the top of the atmosphere (TOA) for the different scenarios described in Section 4. In Section 6, we perform a linear sensitivity analysis on simulated measurements from the OCO spectral regions to get an order of magnitude estimate of the retrieval error in column CO<sub>2</sub> resulting from neglecting polarization. Conclusions for operational retrieval algorithms are drawn in Section 7.

## 2. Digest of vector radiative transfer theory

In the absence of thermal emission, the equation of radiative transfer (RTE) can be written as [25]

$$u \frac{\partial}{\partial \tau} \mathbf{I}(\tau, u, \phi) = \mathbf{I}(\tau, u, \phi) - \mathbf{J}(\tau, u, \phi), \quad (1)$$

where  $\tau$ ,  $u$  and  $\phi$  denote the optical thickness (measured downward from the upper boundary), the cosine of the polar angle (measured from the upward vertical) and the azimuthal angle (measured counterclockwise, looking down, from an arbitrary but fixed direction), respectively. Knowledge of the absolute azimuth angle is not necessary because of rotational symmetry with respect to the vertical axis.  $\mathbf{I}$  is the diffuse (excluding the direct solar beam) radiance vector, which has the Stokes parameters [25]  $I$ ,  $Q$ ,  $U$  and  $V$  as its components. Stokes parameter  $I$  is the intensity,  $Q$  and  $U$  describe the linearly polarized radiation, and  $V$  refers to the circularly polarized radiation. All Stokes parameters have the dimension of radiance and are defined with respect to a reference plane, usually taken to be the local meridian plane. The dependence on wavelength is implicit in this and all subsequent equations. The degree of polarization  $p$  of the radiation is defined as

$$p = \frac{\sqrt{Q^2 + U^2 + V^2}}{I}. \quad (2)$$

The circular polarization can generally be ignored for most atmospheric applications. If the Stokes parameter  $U$  is also equal to zero (or not measured) the following definition of the degree of (linear) polarization is relevant:

$$p = \frac{-Q}{I}. \quad (3)$$

For  $p > 0$ , the radiation is polarized perpendicular to the reference plane. For  $p < 0$ , the radiation is polarized parallel to the reference plane.

The source term  $\mathbf{J}$  has the form

$$\mathbf{J}(\tau, u, \phi) = \frac{\omega(\tau)}{4\pi} \int_{-1}^1 \int_0^{2\pi} \mathbf{P}(u, u', \phi - \phi') \mathbf{I}(\tau, u', \phi') d\phi' du' + \mathbf{Q}(\tau, u, \phi), \quad (4)$$

where  $\omega$  denotes the single scattering albedo (ratio of scattering to extinction optical depth) and  $\mathbf{P}$  is called the phase matrix, which is related to two other matrices called the Mueller matrix and the scattering matrix. The former is the linear transformation connecting the incident and (singly) scattered Stokes vectors in the scattering plane. For scattering by a small volume containing an ensemble of particles, the ensemble-averaged Mueller matrix is called the scattering matrix. When transforming from the scattering plane to the local meridian plane, we obtain the phase matrix. The scattering matrix is normalized such that the average of the phase function (which is the (1,1) matrix element) over all directions is unity. We restrict our attention to scattering matrices of the form considered by Hovenier [26]. This type with only six independent elements is valid in the following situations [27]:

- (1) scattering by an ensemble of randomly oriented particles, each with a plane of symmetry;
- (2) scattering by an ensemble of particles and their mirror particles in equal number and random orientation;
- (3) Rayleigh scattering.

The first term on the right-hand side of Eq. (4) accounts for the integrated scattering of the diffuse light from all directions into the viewing direction and the inhomogeneous term  $\mathbf{Q}$  describes single scattering of the attenuated direct solar beam. This term can be expressed as

$$\mathbf{Q}(\tau, u, \phi) = \frac{\omega}{4\pi} \mathbf{P}(u, -\mu_0, \phi - \phi_0) \mathbf{I}_0 e^{-\tau/\mu_0}, \quad (5)$$

where  $\mu_0 = |u_0|$ ,  $u_0$  is the cosine of the solar zenith angle (SZA),  $\phi_0$  is the solar azimuth and  $\mathbf{I}_0$  is the Stokes vector of the incoming solar beam. This is the standard formulation for a plane-parallel atmosphere.

When Rayleigh scattering and particulate scattering are both present, the effective single scattering albedo  $\omega$  is a weighted sum of the molecular single scattering albedo (which is equal to 1) and the single scattering albedos  $\omega_s$  of the  $s$  aerosol/cloud types

$$\omega = \frac{\tau_r + \sum_s \tau_s \omega_s}{\tau}, \quad (6)$$

where  $\tau_r$  is the Rayleigh scattering optical depth and  $\tau_s$  is the extinction optical depth of the  $s$ th aerosol/cloud type. A similar procedure is used to obtain the effective scattering matrix, except that the normalization here is over the total *scattering* optical depth.

We seek a solution to Eq. (1) subject to the top and bottom boundary conditions (no downwelling diffuse radiance at the TOA and known bidirectional reflectance at the surface) and continuity at the layer interfaces. The total radiance vector is of course the sum of the diffuse and direct components, where the direct radiance vector  $\mathbf{I}^{\text{dir}}$  is given by

$$\mathbf{I}^{\text{dir}}(\tau, u, \phi) = \mathbf{I}_0 e^{-\tau/\mu_0} \delta(u - u_0) \delta(\phi - \phi_0), \quad (7)$$

where  $\delta$  refers to the delta function. The incident solar radiation is assumed to be unidirectional and unpolarized.

### 3. Numerical vector model: VLIDORT

The multiple scattering multi-layer vector discrete ordinate code VLIDORT (developed by Robert Spurr in 2004) was used for all simulations of the Stokes vector. This code is a vector companion to the LIDORT suite of linearized scalar discrete ordinate models [28–31]. In common with other vector codes, including the doubling-adding code of de Haan et al. [32,33] and the VDISORT codes [34,35], VLIDORT uses an analytical Fourier decomposition of the phase matrix [36–38] in order to isolate the azimuthal dependence in the RTE.

For the solution of the homogeneous vector RTE for each Fourier term, VLIDORT follows the formalism of Siewert [39], in which it was demonstrated that full accuracy for homogeneous solutions can only be obtained with the use of a complex-variable eigen-solver module to determine solutions to the coupled linear differential equations. For the inhomogeneous source terms due to scattering of the solar beam, the particular solution is obtained using algebraic substitution methods employing a reduction in the order of the coupled equations. Particular solutions are combined with the real parts of the homogeneous solutions in the boundary value problem to determine the complete Stokes vector field at quadrature (discrete ordinate) polar directions. The numerical integrations are performed using double-Gauss quadrature. Output at user-defined off-quadrature polar angles and arbitrary optical thickness values is obtained using the source function integration technique due to Chandrasekhar [25].

VLIDORT has the ability to calculate the solar beam attenuation (before scattering) in a curved refracting atmosphere, even though the scattering itself is treated for a plane-parallel medium. This is the pseudo-spherical approximation as used in the LIDORT [29] and SDISORT [40] codes, and it enables accurate results to be obtained for SZAs up to  $90^\circ$ . In this paper, we do not consider SZA values greater than  $70^\circ$ , and the plane-parallel source term expression shown in Eq. (5) is sufficient.

VLIDORT was verified through extensive comparisons with existing benchmarks for the one-layer slab problem. For the Rayleigh atmosphere, the tables of Coulson et al. are appropriate [41]. For the slab problem with aerosol sources, Siewert has provided several benchmark results [39] for the discrete ordinate solution; his results have in turn been verified against output from other vector models (see for example [42]).

#### 4. Scenarios for the $O_2 A$ band

The atmosphere is assumed to be plane-parallel, consisting of homogeneous layers, each of which contains gas molecules and aerosols (there is no aerosol in the top two layers). We use 11 layers (see Table 1) with the altitudes and level temperatures corresponding to the 1976 US standard model atmosphere [43]. The top four layers are in the stratosphere, with the rest in the troposphere. Since oxygen is a well-mixed gas throughout most of the atmosphere, a constant volume mixing ratio of 0.209476 was assumed [44]. The spectroscopic data were taken from the HITRAN2K line list [45]. The aerosol types in the planetary boundary layer (lowest two layers) and free troposphere (next five layers) have been chosen to correspond to the urban and tropospheric models developed by Shettle and Fenn [46], with an assumption of moderate humidity (70%). For the stratosphere, in correspondence with standard practice, a 75% solution of  $H_2SO_4$  was assumed with a modified gamma size distribution [47]. The complex refractive index of the sulfuric acid solution was taken from the tables prepared by Palmer and Williams [48]. The single scattering properties for the above aerosol

Table 1  
Model atmosphere

Level	Altitude (km)	Pressure (mbar)	Temperature (K)
0	50.0	$7.798 \times 10^{-1}$	270.7
1	40.0	$2.871 \times 10^0$	250.4
2	30.0	$1.197 \times 10^1$	226.5
3	20.0	$5.529 \times 10^1$	216.7
4	12.0	$1.940 \times 10^2$	216.7
5	10.0	$2.650 \times 10^2$	223.3
6	8.0	$3.565 \times 10^2$	236.2
7	6.0	$4.722 \times 10^2$	249.2
8	4.0	$6.166 \times 10^2$	262.2
9	2.0	$7.950 \times 10^2$	275.2
10	1.0	$8.988 \times 10^2$	281.7
11	0.0	$1.013 \times 10^3$	288.2

The altitude, pressure and temperature are level quantities. The corresponding layer values are assumed to be the mean of the values at the levels bounding the layer.

types were computed using a Mie scattering code [49] that generates coefficients for the expansion in generalized spherical functions. The atmosphere is bounded below by a lambertian reflecting surface. Computations were done for SZAs of  $10^\circ$ ,  $40^\circ$  and  $70^\circ$ , viewing zenith angles of  $0^\circ$ ,  $35^\circ$  and  $70^\circ$  and relative azimuth angles of  $0^\circ$ ,  $45^\circ$ ,  $90^\circ$ ,  $135^\circ$  and  $180^\circ$ . Variations in surface reflectance (0.05, 0.1 and 0.3) and aerosol extinction optical depth (0, 0.0247 and 0.247) have also been considered. The baseline case corresponds to a surface reflectance and aerosol extinction optical depth of 0.3 and 0.0247, respectively.

Fig. 1 shows the total molecular absorption optical depth (solid line), shown at high (line-by-line) spectral resolution, the Rayleigh scattering optical depth (dotted line) and the aerosol extinction optical depth (dashed line) of the 11-layer atmosphere (for the baseline case) as a function of wavelength in the  $O_2 A$  band. Aerosol scattering has been assumed to be invariant in wavelength, which is a good approximation over the width of a molecular absorption band. It can be seen that while the Rayleigh scattering is also fairly constant, the molecular absorption shows strong variations with wavelength.

Fig. 2 shows the aerosol vertical profile for the baseline case. Changing the aerosol extinction optical depth corresponds to applying a scaling factor to the above profile. The aerosol scattering phase function  $F_{11}$  and the degree of linear polarization (for unpolarized incident light)  $-F_{21}/F_{11}$  for the urban aerosol are plotted in Fig. 3, alongwith the corresponding plots for Rayleigh scattering. The other aerosol types exhibit similar behavior, with the major difference being the single scattering albedos. The diffraction forward peak is clearly visible. Twice refracted rays account for much of the forward scattering. The negative polarization peak at about  $160^\circ$  is the rainbow, caused by internal reflection. The enhanced intensity in the backscattering direction is the glory. Although aerosol particles are less polarizing than air molecules, the scattering optical depth for aerosols is typically 5–6 times the Rayleigh scattering optical depth in this part of the near infrared; polarization effects in the  $O_2 A$  band are therefore not straightforward to delineate.

Intensity and polarization spectra are shown in Fig. 4 for a case with SZA, viewing zenith angle and relative azimuth angle equal to  $40^\circ$ ,  $35^\circ$  and  $180^\circ$ , respectively. The surface reflectance and aerosol extinction optical depth correspond to the baseline scenario.

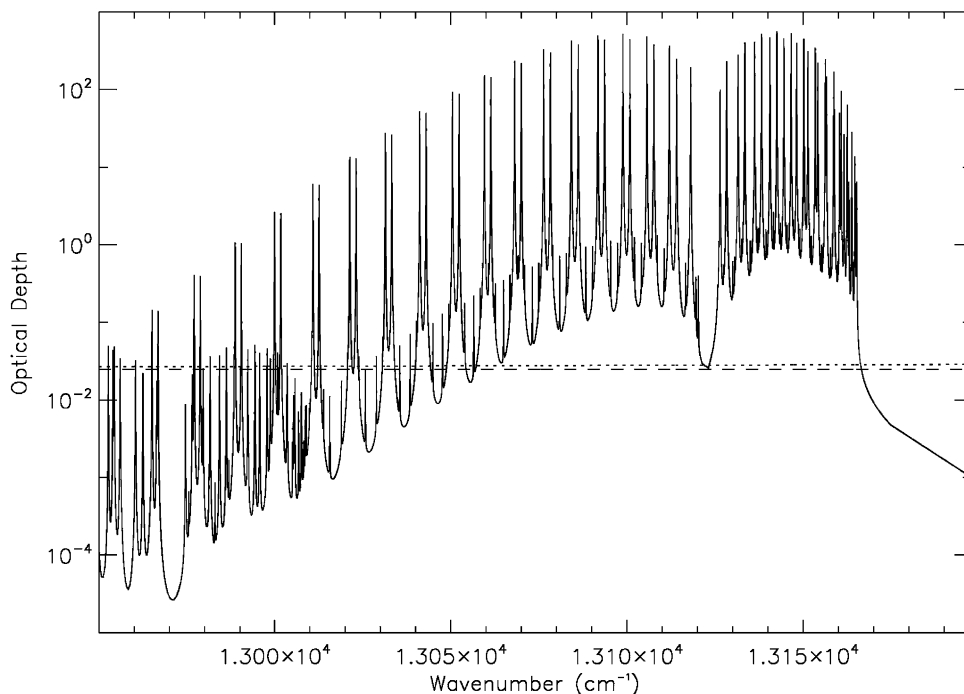


Fig. 1. Molecular absorption optical depth (solid line), Rayleigh scattering optical depth (dotted line) and aerosol extinction optical depth (dashed line) of the model atmosphere.

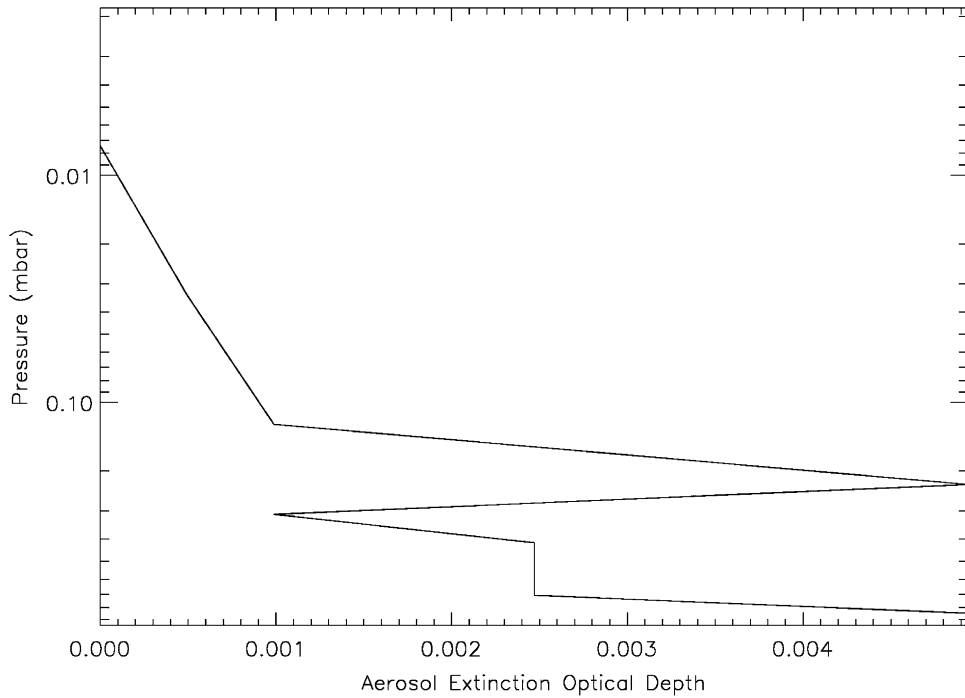


Fig. 2. Aerosol vertical profile.

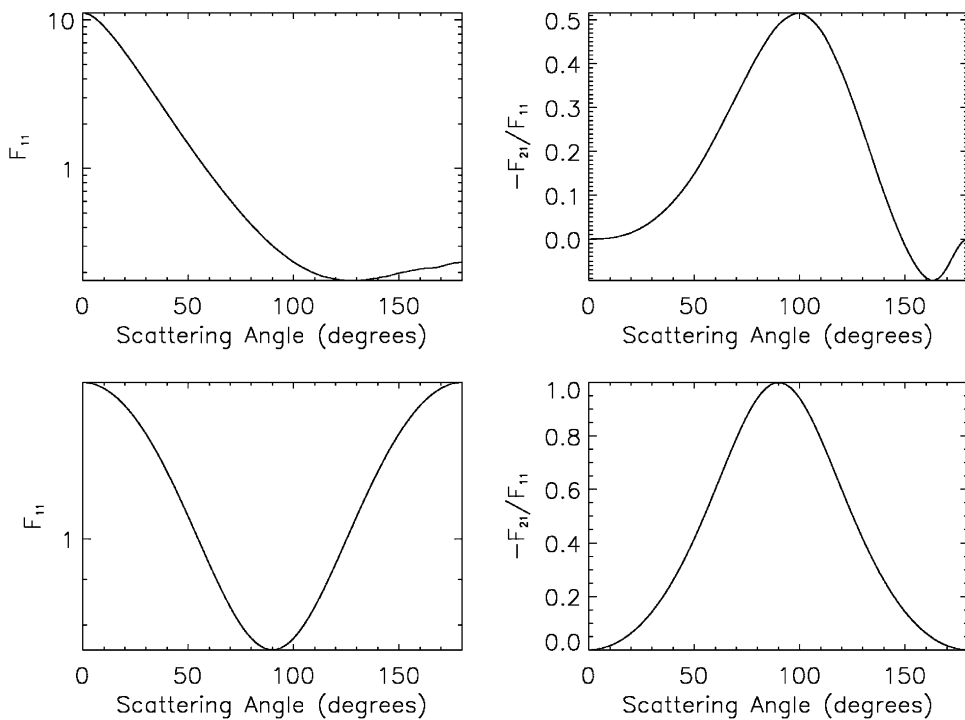


Fig. 3. (Top row, left to right) aerosol scattering phase function and degree of linear polarization; (bottom row, left to right) Rayleigh scattering phase function and degree of linear polarization.

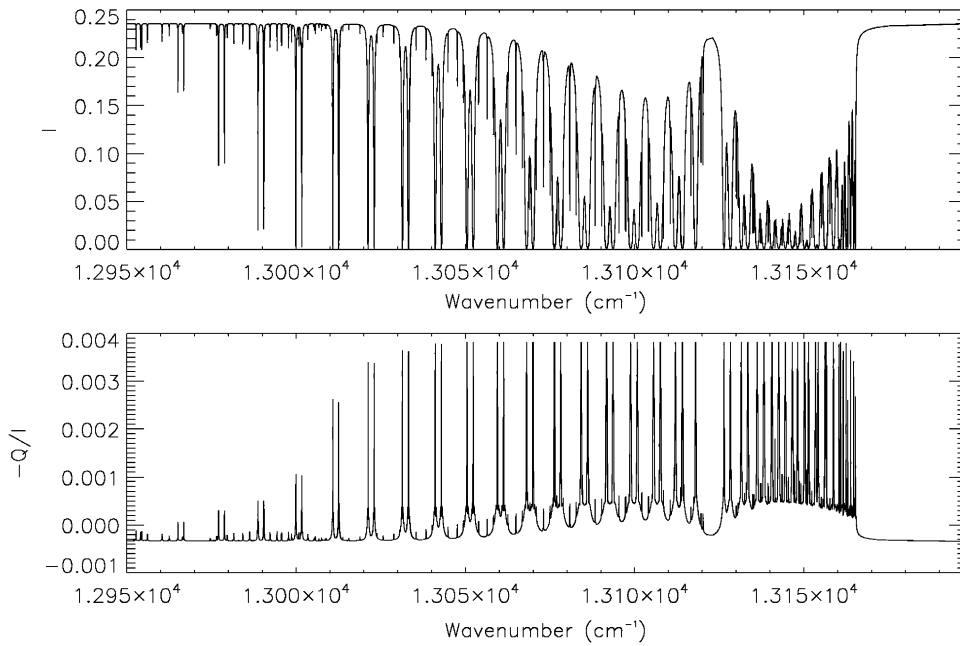


Fig. 4. Intensity (top) and polarization (bottom) spectra of the  $O_2 A$  band. The SZA, viewing zenith angle and relative azimuth angle are  $40^\circ$ ,  $35^\circ$  and  $180^\circ$ , respectively. The surface reflectance and aerosol extinction optical depth are 0.3 and 0.0247, respectively.

## 5. Results

Before discussing the results, it is necessary to define the error plotted in Figs. 5–8. The OCO instrument is designed to measure only the radiation perpendicular to the plane containing the incoming solar beam and the beam entering the instrument, i.e.  $I - Q$ . Neglecting polarization in the RT computations thus creates a disparity between calculation and measurement. The error made by a scalar approximation can be expressed as

$$Error = \frac{I_s - (I - Q)}{I - Q} \times 100, \quad (8)$$

where the subscript  $s$  denotes a scalar computation. It is more instructive to rewrite the above equation in the following manner:

$$Error = \left( \frac{(I_s/I)}{1 - (Q/I)} - 1 \right) \times 100. \quad (9)$$

Clearly, the error is influenced by errors in the intensity and degree of linear polarization. However, calculations show that the error in the intensity is for most practical cases less than 0.5%. It is not insignificant only in the case of extremely high aerosol loading and even then only in the continuum (where the total error is much lower than in the absorption line cores). For this reason, plots of  $I_s/I$  are not shown, though the plotted error takes into account this factor. Generally, greater polarization induces greater error. From the above definition, it is clear that scalar–vector errors will be larger when the radiation is polarized parallel to the reference plane. Even a 100% positive polarization creates only a 50% error (assuming no error in the intensity), but the error can grow beyond limit if the polarization is highly negative. This is a clear consequence of measuring only the perpendicularly polarized radiation.

In Fig. 5, the rows represent, from top to bottom, gas absorption optical depths of 0.000113, 0.818 and 103.539, respectively. These characterize the three different regimes of interest pointed out by Stam et al. [23], viz., the continuum, an intermediate region and the core of a very strong line in the  $O_2 A$  band. The columns

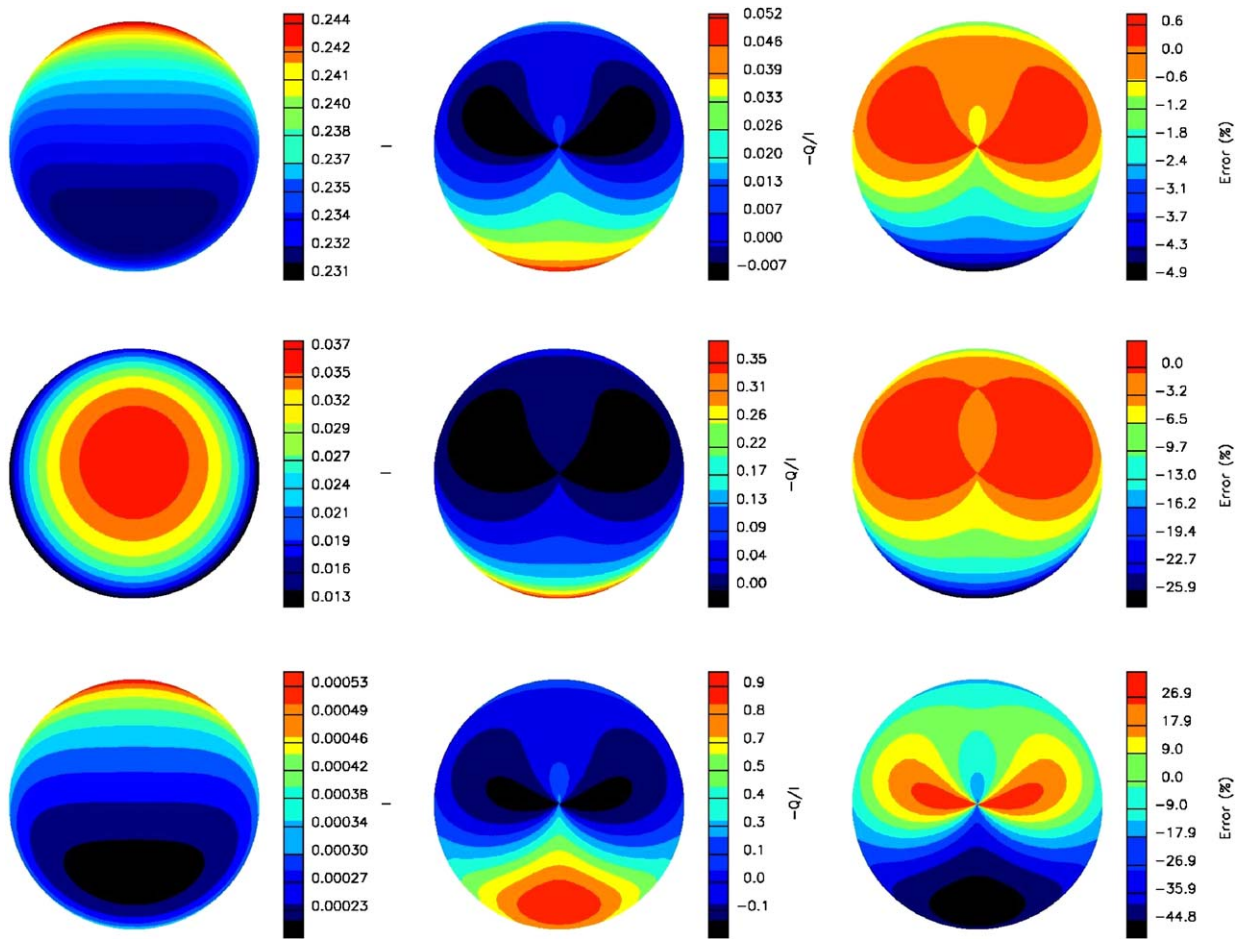


Fig. 5. Orthographic plots showing variation of intensity (left column), linear polarization (middle column) and error if polarization is neglected (right column) for gas absorption optical depths of 0.000113 (top row), 0.818 (middle row) and 103.539 (bottom row). The viewing angle increases radially from  $0^\circ$  to  $70^\circ$  and the relative azimuth angle increases anticlockwise from  $0^\circ$  at the nadir position, with zenith representing  $180^\circ$ . The SZA, surface reflectance and aerosol extinction optical depth are  $40^\circ$ , 0.3 and 0, respectively.

are, from left to right, the intensity  $I$ , the degree of linear polarization  $-Q/I$  and the percentage error if polarization is neglected, respectively. In all the orthographic projections, the viewing zenith angle increases radially outward from  $0^\circ$  to  $70^\circ$  while the relative azimuth angle increases anticlockwise from  $0^\circ$  at the nadir position. The zenith position represents an angle of  $180^\circ$ . The SZA and viewing zenith angle were not increased beyond  $70^\circ$  to avoid complications due to curvature of the beam paths.

The line core behavior corresponds to single scattering in a Rayleigh atmosphere. The absorption is too strong for photons to hit the surface. The intensity and polarization depend only on the scattering angle and, in the case of the latter, the angle between the scattering and meridional planes. As the gas absorption optical depth decreases, photons penetrate more and more of the atmosphere until they hit the surface and bounce back. The lambertian nature of the surface randomizes the orientation of the reflected beam and reduces polarization. The intensity, on the other hand, increases because, unlike for the line cores, light is reflected back from the surface in addition to being scattered by the air molecules.

In Figs. 6–8 the same quantities are plotted as in Fig. 4, except that only the variation in the principal plane is shown. Negative viewing angles correspond to a relative azimuth angle of  $180^\circ$ . In Fig. 6, the SZA is varied, with the aerosol extinction optical depth and surface reflectance fixed at 0.0247 and 0.3, respectively. The solid,

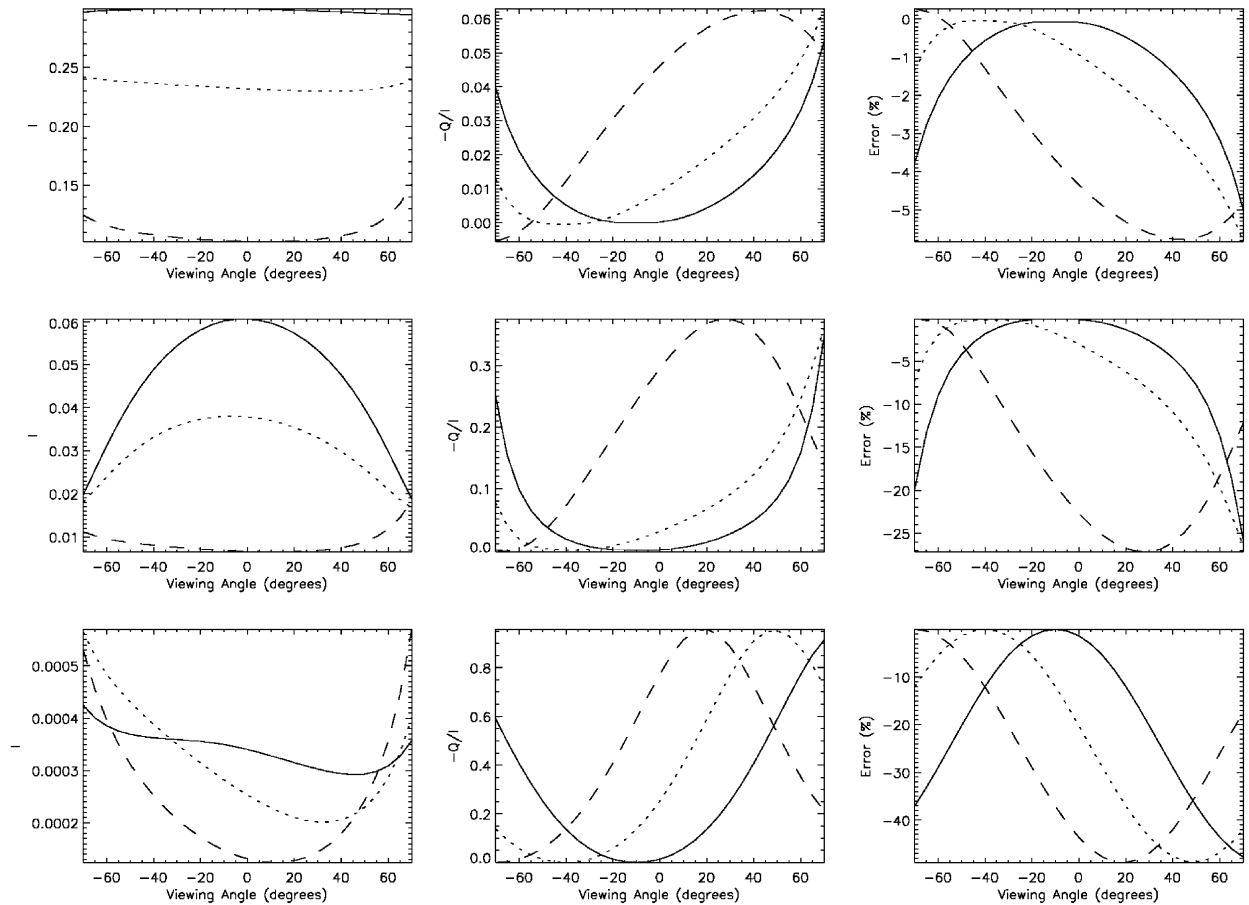


Fig. 6. Variation of intensity (left column), linear polarization (middle column) and error if polarization is neglected (right column) for gas absorption optical depths of 0.000113 (top row), 0.818 (middle row) and 103.539 (bottom row) as a function of viewing angle in the principal plane. Positive viewing angles are for a relative azimuth angle of  $0^\circ$  while negative viewing angles are for a  $180^\circ$  relative azimuth angle. Solid, dotted and dashed lines represent SZAs of  $10^\circ$ ,  $40^\circ$  and  $70^\circ$ , respectively. The surface reflectance and aerosol extinction optical depth are 0.3 and 0.0247, respectively.

dotted and dashed lines correspond to SZAs of  $10^\circ$ ,  $40^\circ$  and  $70^\circ$ , respectively. At the continuum, the intensity decreases as the SZA increases because of greater attenuation of the direct beam. The polarization, on the other hand, increases because less light reaches the surface and its depolarizing effect is reduced. The net result is that the error increases. Departures from this general trend are due to the predominance of single scattering (as opposed to multiple scattering) for certain viewing geometries, as described in Stam et al. [23]. The behavior in the line cores is more complicated, being driven by single scattering, and thus the geometry.

As the aerosol loading increases (Fig. 7), the intensity increases in the line core due to greater scattering while the polarization decreases because the aerosol is less polarizing than air molecules. The behavior is more complicated in the continuum, where there are contributions from reflected light from the surface and multiply scattered light from the atmosphere. Increasing the aerosol loading increases the total extinction depth and causes more multiple scattering. The former reduces the number of photons reaching the surface, resulting in less light being reflected back. The latter has the opposite effect. Depending on which effect is stronger, the intensity can increase or decrease. A similar argument could be made for the polarization.

Finally, the surface reflectance has no effect in the line cores, where light does not reach the surface (Fig. 8). Decreasing the reflectance lowers the continuum brightness, because less light is reflected from the surface, and increases the polarization because of reduced contribution from the surface relative to the atmosphere.

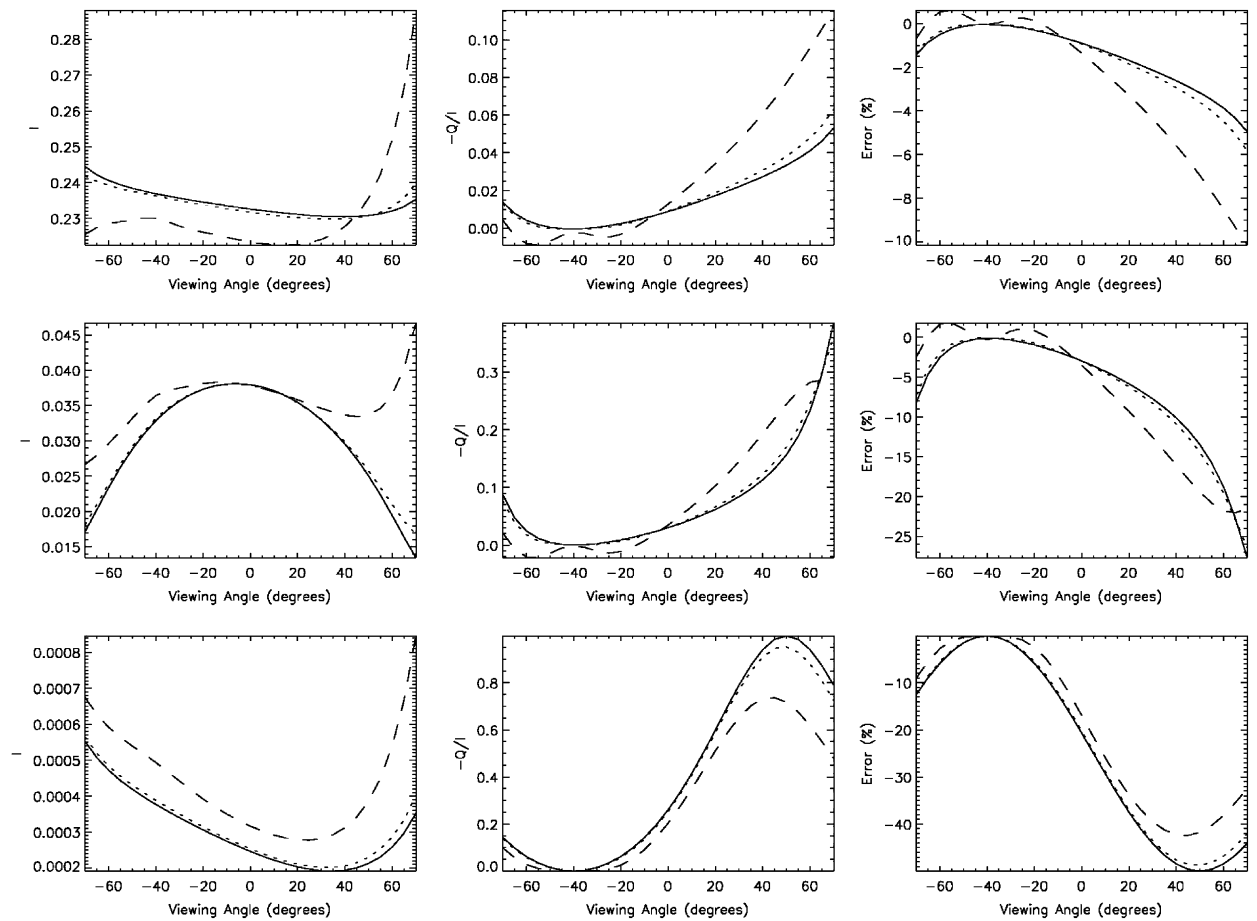


Fig. 7. Same as Fig. 6 except that the SZA is  $40^\circ$  and the solid, dotted and dashed lines represent aerosol extinction optical depths of 0, 0.0247 and 0.247, respectively.

The lambertian nature of the surface also results in greater angular variation in both the intensity and polarization at lower reflectances. This is again in agreement with the results from Stam et al. [23].

Though we have not considered non-lambertian surfaces, a short discussion is in order. In the case of polarizing surfaces  $Q/I$  in the continuum will increase relative to the lambertian surface case because light can penetrate to the surface. Inside the absorption bands, the increase in  $Q/I$  will be lower. Therefore the difference between  $Q/I$  in and outside the absorption bands will decrease, making the errors due to a scalar approximation smaller.

Clearly, the most pathological case is that of a Rayleigh scattering atmosphere bounded by a lambertian surface with extremely low reflectance, with the sun at a very low elevation. It is worthwhile to note that all the above conclusions are based on line-by-line calculations. Convolution with a typical instrument response function could reduce the errors significantly.

## 6. Linear sensitivity analysis

It is important to recognize that what we really need to know for the OCO mission is the effect of neglecting polarization when translated to errors in the retrieved  $\text{CO}_2$  column. These errors can be assessed by performing a linear error analysis study [50]. In general, linear error analysis allows quantification of errors caused by uncertainties in the forward model parameters, i.e. parameters that are not retrieved, or by inadequacies in the forward model itself (forward model errors), such as neglecting polarization. Forward

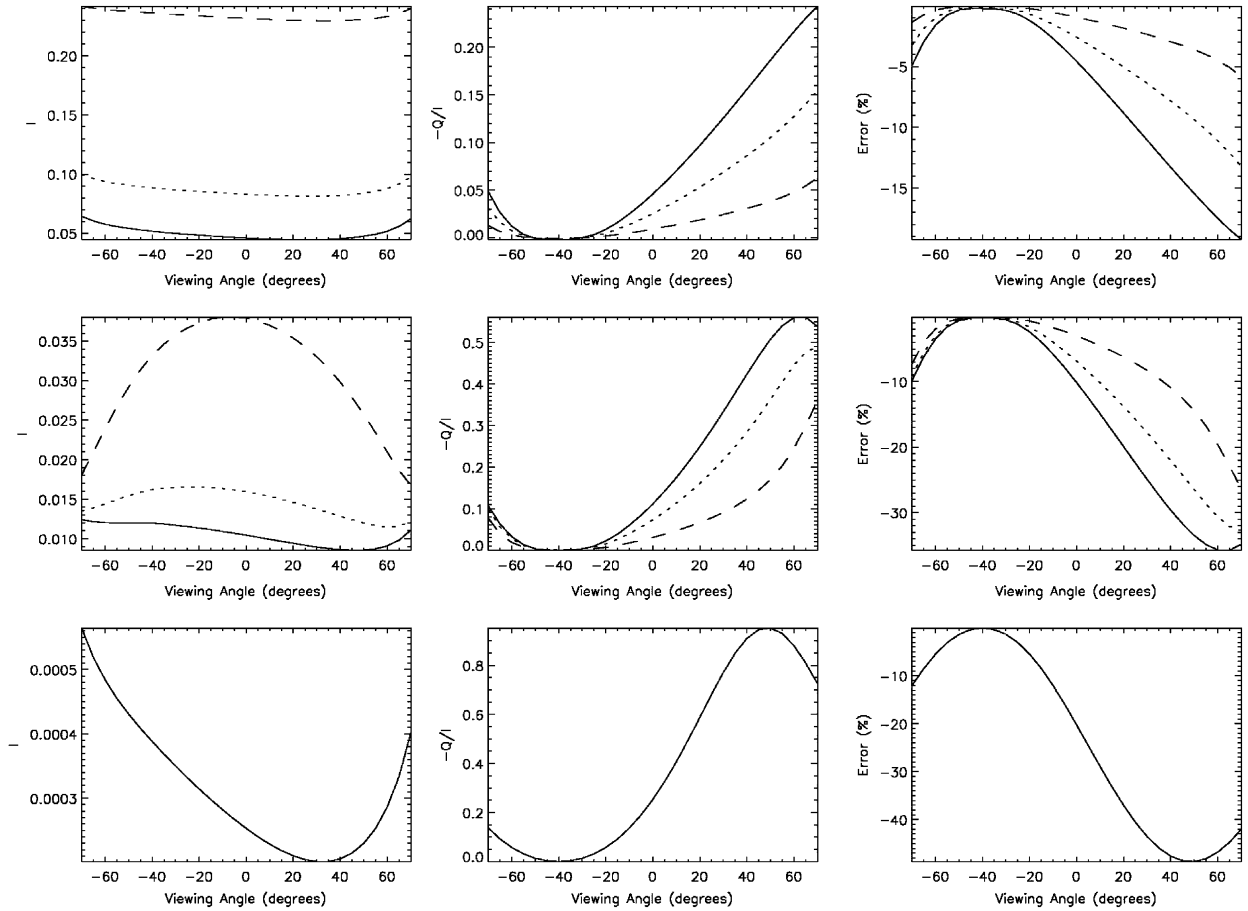


Fig. 8. Same as Fig. 6 except that the SZA is 40° and the solid, dotted and dashed lines represent surface reflectances of 0.05, 0.1 and 0.3, respectively.

model errors are typically systematic and result in a bias in the retrieved parameters  $\mathbf{x}$ . This bias can be expressed as

$$\Delta \mathbf{x} = \mathbf{G} \Delta \mathbf{F}, \tag{10}$$

where  $\mathbf{G}$  is the gain matrix that represents the mapping of the measurement variations into the retrieved vector variations and  $\Delta \mathbf{F}$  is the error in the modeling made by the scalar approximation

$$\Delta \mathbf{F} = (\mathbf{I} - \mathbf{Q}) - \mathbf{I}_s, \tag{11}$$

where  $\mathbf{I}$ ,  $\mathbf{Q}$  and  $\mathbf{I}_s$  are as defined before except that they are vectors over the detector pixels.

The linear error analysis was carried out with the OCO Level 2 retrieval algorithm. This algorithm has been developed to retrieve the column-averaged dry air mole fraction of CO<sub>2</sub> from space-based measurements of the OCO spectral bands [51]. The retrieval algorithm iteratively adjusts a set of atmospheric/surface/instrument parameters by alternate calls to a forward model and an inverse method. The forward model computes a high spectral resolution, monochromatic, TOA radiance spectrum. Repeated calls to the scalar RT code Radiant [52] are used to generate the spectrum. The calculated spectrum is then convolved with the OCO instrument lineshape, which has been assumed to be Lorentzian with resolving powers of 17 000 for the O<sub>2</sub> A band and 20 000 for the CO<sub>2</sub> bands, respectively. The inverse method is based on optimal estimation [50] and uses a priori information to constrain the retrieval problem. Weighting functions describing the change of the

Table 2  
Retrieval and smoothing errors and errors from neglecting polarization for January and July scenes in Park Falls, WI, USA

Scenario	Retrieval error (ppm)	Polarization error (ppm)	Smoothing error (ppm)
January	1.8	7.4	1.0
July	0.4	0.4	0.1

measured spectrum with respect to a change in the retrieved parameters are calculated using finite differences. The OCO algorithm simultaneously fits the spectra of the three absorption bands, each containing  $\sim 900$  spectral points, and retrieves a set of 61 parameters for a 12-level atmosphere. These retrieved parameters are the vertical profiles of CO<sub>2</sub> vmr, H<sub>2</sub>O vmr, temperature, aerosol optical depth as well as surface pressure, surface reflectance and its spectral dependence, spectral shift and squeeze/stretch. The a priori covariance for CO<sub>2</sub> has been computed using the MATCH/CASA model [53], scaled to obtain a column variability of about 4.6 ppm to avoid over-constraining the retrieval. For all other retrieval parameters, ad hoc constraints have been used, with no cross-correlation between different parameters.

We simulated nadir OCO spectra for Park Falls, WI, USA, for January (SZA = 75.1°) and July (SZA = 34.8°). Temperature and humidity profiles and surface pressure were taken from the ECMWF ERA-40 dataset [54] and CO<sub>2</sub> profiles from the MATCH/CASA model calculations. For the January and July scenes, we assumed complete snow cover and conifer vegetation, respectively. The calculation was carried out for a total aerosol optical depth of 0.1 using the aerosol types given in Section 4. Signal-to-noise ratios of 360, 250 and 180 were used for the O<sub>2</sub> A band, the 1.61  $\mu\text{m}$  CO<sub>2</sub> band and the 2.06  $\mu\text{m}$  CO<sub>2</sub> band, respectively. We applied the retrieval algorithm to the simulated spectra starting with the known, true solution, i.e. we assumed that the iterative retrieval scheme had already converged. The retrieval and smoothing errors and the gain matrix are calculated by the retrieval algorithm. The smoothing error describes the error in the retrieved parameters due to the limited sensitivity of the retrieval to fine-structures of atmospheric profiles. The analysis of smoothing errors requires knowledge about the real atmospheric variability; we calculated the CO<sub>2</sub> covariance using the MATCH/CASA model and scaled it to approximate a 2 ppm column variability observed from aircraft measurements [55]. The error in the radiance made by the scalar approximation  $\Delta F$  was computed using VLIDORT for the same two scenarios. Errors due to the usage of two different RT codes are negligible. VLIDORT (when run in scalar mode) and Radiant agree to five decimal places or better for the intensities, and generally four significant figures for the weighting functions.

The obtained retrieval and smoothing errors and the error due to neglecting polarization are summarized in Table 2. We found that in July the largest error was the retrieval error; the smoothing error was negligible and the error due to neglecting polarization was comparable to the retrieval error. On the other hand, for the January scenario, the error caused by ignoring polarization was the dominant error term; it was roughly 4 times the retrieval error and 7 times the smoothing error. Most real scenarios might be expected to fall in between these extremes. Considering that the required CO<sub>2</sub> retrieval precision for OCO is  $\sim 2$  ppm, it is evident that polarization will play a significant role in the error budget. Also, as shown in Figs. 5, 6 and 8, the effect of neglecting polarization depends on the surface reflectance and measurement geometry and is hence likely to result in a regionally varying bias in the retrieved CO<sub>2</sub> columns. As pointed out by Rayner and O'Brien [56], it is critical to avoid such a bias since it will give rise to large systematic errors in a subsequent inversion for carbon sources and sinks.

## 7. Conclusions

Sensitivity studies were performed to evaluate the errors resulting from ignoring polarization in simulations of backscatter measurements of the O<sub>2</sub> A band by space-based instruments such as that on OCO. Beam and viewing geometry, surface reflectance and aerosol loading were systematically varied. Different behavior was observed in the line cores and the continuum because of the different paths taken by the photons in the two

cases. The maximum errors were found for a Rayleigh scattering atmosphere bounded by a poorly reflecting lambertian surface, when illuminated by a low sun.

A linear error analysis study of simulated measurements from the OCO absorption bands showed that neglecting polarization could introduce errors as high as 10 ppm, which is substantially larger than the required retrieval precision of  $\sim 2$  ppm. The retrieval error budget could thus be potentially dominated by polarization. On the other hand, it is impractical to do full vector retrievals because of the computational cost. It is thus imperative to find ways to minimize the error without actually doing a complete Stokes vector calculation.

There are a variety of approaches to save time compared to a full vector calculation and get more accurate results than if polarization were ignored. Since multiple scattering tends to remove polarization features, the Stokes parameters  $Q$  and  $U$  could be computed using one or two orders of scattering (which take negligible time), with a correction for the intensity such as that proposed by Sromovsky [57]. Alternatively, one could use spectral binning (see, e.g. [58], for a scalar case) to reduce the number of RT calculations. Another possibility is to create lookup tables for a wide variety of scenarios and simply use them to interpolate for intermediate scenarios.

## Acknowledgments

This work was supported in part by NASA Grant NAG1-1806 and the Orbiting Carbon Observatory (OCO) Project at JPL. We would like to thank Joop Hovenier and Johan de Haan for providing us with a doubling-adding vector RT code to verify the results from VLIDORT. We would also like to acknowledge David Crisp, Run-Lie Shia, Jack Margolis and Xin Guo for reviewing the manuscript, and Charles Miller, Geoff Toon and Bhaswar Sen for helpful comments.

## References

- [1] O'Brien DM, English SA, da Costa GA. High-precision, high-resolution measurements of absorption in the oxygen A-band. *J Atmos Ocean Technol* 1997;14(1):105–19.
- [2] O'Brien DM, Mitchell RM, English SA, da Costa GA. Airborne measurements of air mass from O<sub>2</sub> A-band absorption spectra. *J Atmos Ocean Technol* 1998;15(6):1272–86.
- [3] O'Brien DM, Mitchell RM. Error estimates for retrieval of cloud-top pressure using absorption in the A band of oxygen. *J Appl Meteorol* 1992;31(10):1179–92.
- [4] Kuze A, Chance KV. Analysis of cloud top height and cloud coverage from satellite using the O<sub>2</sub> A and B bands. *J Geophys Res* 1994;99(D7):14481–92.
- [5] Koelemeijer RBA, Stammes P, Hovenier JW, de Haan JF. A fast method for retrieval of cloud parameters using oxygen A band measurements from the global ozone monitoring experiment. *J Geophys Res* 2001;106(D4):3475–90.
- [6] Rozanov VV, Kokhanovsky AA. Semianalytical cloud retrieval algorithm as applied to the cloud top altitude and the cloud geometrical thickness determination from top-of-atmosphere reflectance measurements in the oxygen A band. *J Geophys Res* 2004;109(D5):D05202.
- [7] Rozanov VV, Kokhanovsky AA, Burrows JP. The determination of cloud altitudes using GOME reflectance spectra: multilayered cloud systems. *IEEE Trans Geosci Remote Sensing* 2004;42(5):1009–17.
- [8] Jiang Y, Yung YL, Sander SP, Travis LD. Modeling of atmospheric radiative transfer with polarization and its application to the remote sensing of tropospheric ozone. *JQSRT* 2004;84(2):169–79.
- [9] Hasekamp OP, Landgraf J. Tropospheric ozone information from satellite-based polarization measurements. *J Geophys Res* 2002;107(D17):4326.
- [10] Hasekamp OP, Landgraf J, van Oss R. The need of polarization modeling for ozone profile retrieval from backscattered sunlight. *J Geophys Res* 2002;107(D23):4692.
- [11] Liu X, Chance K, Sioris CE, Spurr RJD, Kurosu TP, Martin RV, Newchurch MJ. Ozone profile and tropospheric ozone retrievals from the Global Ozone Monitoring Experiment: algorithm description and validation. *J Geophys Res* 2005;110(D20):D20307.
- [12] Takano Y, Liou KN. Solar radiative transfer in cirrus clouds. Part I: single-scattering and optical properties of hexagonal ice crystals. *J Atmos Sci* 1989;46(1):3–19.
- [13] Takano Y, Liou KN. Solar radiative transfer in cirrus clouds. Part II: theory and computation of multiple scattering in an anisotropic medium. *J Atmos Sci* 1989;46(1):20–36.
- [14] Takano Y, Liou KN. Radiative transfer in cirrus clouds. Part III: light scattering by irregular ice crystals. *J Atmos Sci* 1995;52(7):818–37.

- [15] Mishchenko MI, Travis LD. Satellite retrieval of aerosol properties over the ocean using polarization as well as intensity of reflected sunlight. *J Geophys Res* 1997;102(D14):16989–7014.
- [16] Deuze JL, Goloub P, Herman M, Marchand A, Perry G, Susana S, et al. Estimate of the aerosol properties over the ocean with POLDER. *J Geophys Res* 2000;105(D12):15329–46.
- [17] Levy RC, Remer LA, Kaufman YJ. Effects of neglecting polarization on the MODIS aerosol retrieval over land. *IEEE Trans Geosci Remote Sensing* 2004;42(11):2576–83.
- [18] Jiang Y, Jiang X, Shia RL, Sander SP, Yung YL. Polarization study of the O<sub>2</sub> A-band and its application to the retrieval of O<sub>2</sub> column abundance. *EOS Trans Am Geophys Union* 2003;84(46):A41E-0735 255.
- [19] Knibbe WJJ, de Haan JF, Hovenier JW, Stam DM, Koelemeijer RB, Stammes P. Deriving terrestrial cloud top pressure from photopolarimetry of reflected light. *JQSRT* 2000;64(2):173–99.
- [20] Schutgens NAJ, Stammes P. Parametrisation of Earth's polarisation spectrum in the ultra-violet. *JQSRT* 2002;75(2):239–55.
- [21] Krijger JM, Tilstra LG. Current status of SCIAMACHY polarisation measurements. Proceedings of the Envisat validation workshop, Frascati, Italy; 2002.
- [22] Tilstra LG, Acarreta JR, Krijger JM, Stammes P. Verification of SCIAMACHY's polarisation correction over the Sahara desert. Proceedings of the Envisat validation workshop, Frascati, Italy; 2002.
- [23] Stam DM, de Haan JF, Hovenier JW, Stammes P. Degree of linear polarization of light emerging from the cloudless atmosphere in the oxygen A band. *J Geophys Res* 1999;104(D14):16843–58.
- [24] Crisp D, Atlas RM, Breon FM, Brown LR, Burrows JP, Ciais P, et al. The orbiting carbon observatory (OCO) mission. *Adv Space Res* 2004;34(4):700–9.
- [25] Chandrasekhar S. Radiative transfer. New York: Dover; 1960.
- [26] Hovenier JW. Multiple scattering of polarized light in planetary atmospheres. *Astron Astrophys* 1971;13:7–29.
- [27] Hovenier JW, van der Mee CVM. Fundamental relationships relevant to the transfer of polarized light in a scattering atmosphere. *Astron Astrophys* 1983;128(1):1–16.
- [28] Spurr RJD, Kurosu TP, Chance KV. A linearized discrete ordinate radiative transfer model for atmospheric remote sensing retrieval. *JQSRT* 2001;68(6):689–735.
- [29] Spurr RJD. Simultaneous derivation of intensities and weighting functions in a general pseudo-spherical discrete ordinate radiative transfer treatment. *JQSRT* 2002;75(2):129–75.
- [30] Spurr RJD. A new approach to the retrieval of surface properties from earthshine measurements. *JQSRT* 2004;83(1):15–46.
- [31] Spurr RJD. LIDORT V2PLUS: a comprehensive radiative transfer package for UV/VIS/NIR nadir remote sensing; a general quasi-analytic solution. Proceedings of the SPIE international symposium, vol. 5235; 2003. p. 89–100.
- [32] de Haan JF, Bosma PB, Hovenier JW. The adding method for multiple scattering calculations of polarized light. *Astron Astrophys* 1987;183(2):371–91.
- [33] Stammes P, de Haan JF, Hovenier JW. The polarized internal radiation field of a planetary atmosphere. *Astron Astrophys* 1989;225(1):239–59.
- [34] Schulz FM, Stammes K, Weng F. VDISORT: an improved and generalized discrete ordinate method for polarized (vector) radiative transfer. *JQSRT* 1999;61(1):105–22.
- [35] Schulz FM, Stammes K. Angular distribution of the Stokes vector in a plane-parallel, vertically inhomogeneous medium in the vector discrete ordinate transfer (VDISORT) model. *JQSRT* 2000;65(4):609–20.
- [36] Siewert CE. On the equation of transfer relevant to the scattering of polarized light. *Astrophys J* 1981;245:1080–6.
- [37] Siewert CE. On the phase matrix basic to the scattering of polarized light. *Astron Astrophys* 1982;109:195–200.
- [38] Vestrucci P, Siewert CE. A numerical evaluation of an analytical representation of the components in a Fourier decomposition of the phase matrix for the scattering of polarized light. *JQSRT* 1984;31(2):177–83.
- [39] Siewert CE. A discrete-ordinates solution for radiative-transfer models that include polarization effects. *JQSRT* 2000;64(3):227–54.
- [40] Dahlback A, Stammes K. A new spherical model for computing the radiation field available for photolysis and heating at twilight. *Planet Space Sci* 1991;39(5):671–83.
- [41] Coulson KL, Dave JV, Sekera Z. Tables related to radiation emerging from a planetary atmosphere with Rayleigh scattering. Berkeley: University of California Press; 1960.
- [42] Wauben WMF, Hovenier JW. Polarized radiation of an atmosphere containing randomly-oriented spheroids. *JQSRT* 1992;47(6):491–504.
- [43] US standard atmosphere. Washington DC: US Government Printing Office; 1976.
- [44] McClatchey RA, Fenn RW, Selby JEA, Volz FE, Garing JS. Optical properties of the atmosphere. Technical Report, AFCRL-72.0497, Air Force Cambridge Research Laboratory, Hanscom Air Force Base, MA; 1972.
- [45] Rothman LS, Barbe A, Benner DC, Brown LR, Camy-Peyret C, Carleer MR, et al. The HITRAN molecular spectroscopic database: edition of 2000 including updates through 2001. *JQSRT* 2003;82(1):5–44.
- [46] Shettle EP, Fenn RW. Models for the aerosols of the lower atmosphere and the effects of humidity variations on their optical properties. Technical Report, AFGL-TR-79-0214, Air Force Geophysics Laboratory, Hanscom Air Force Base, MA; 1979.
- [47] <<http://www.eumetcal.org/euromet/english/satmet/s2400/s240009d.htm>>.
- [48] Palmer KF, Williams D. Optical constants of sulfuric acid; application to the clouds of Venus? *Appl Opt* 1975;14(1):208–19.
- [49] de Rooij WA, van der Stap CCAH. Expansion of Mie scattering matrices in generalized spherical functions. *Astron Astrophys* 1984;131(2):237–48.
- [50] Rodgers CD. Inverse methods for atmospheric sounding: theory and practice. Singapore: World Scientific; 2000.

- [51] Kuang Z, Margolis JS, Toon GC, Crisp D, Yung YL. Spaceborne measurements of atmospheric CO<sub>2</sub> by high-resolution NIR spectrometry of reflected sunlight: an introductory study. *Geophys Res Lett* 2002;29(15):1716.
- [52] Christi MJ, Stephens GL. Retrieving profiles of atmospheric CO<sub>2</sub> in clear sky and in the presence of thin cloud using spectroscopy from the near and thermal infrared: a preliminary case study. *J Geophys Res* 2004;109(D4):D04316.
- [53] Olsen SC, Randerson JT. Differences between surface and column atmospheric CO<sub>2</sub> and implications for carbon cycle research. *J Geophys Res* 2004;109(D2):D02301.
- [54] <<http://data.ecmwf.int/data/d/era40/>>.
- [55] Tans PP, et al. Carbon cycle. In: Hoffman DJ, Peterson JT, Rosson RM, editors. *Climate monitoring and diagnostics laboratory*, vol. 23, Summary report 1994–1995. Boulder: US Department of Commerce; 1996.
- [56] Rayner PJ, O'Brien DM. The utility of remotely sensed CO<sub>2</sub> concentration data in surface source inversions. *Geophys Res Lett* 2001;28(1):175–8.
- [57] Stromovsky LA. Effects of Rayleigh-scattering polarization on reflected intensity: a fast and accurate approximation method for atmospheres with aerosols. *Icarus* 2005;173(1):284–94.
- [58] Meadows VS, Crisp D. Ground-based near-infrared observations of the Venus nightside: the thermal structure and water abundance near the surface. *J Geophys Res* 1996;101(E2):4595–622.